

Kinematics of τ two-body decay near τ threshold at BESIII*

MO Xiao-Hu(莫晓虎)¹⁾

Institute of High Energy Physics, CAS, Beijing 100049, China

Abstract The kinematic properties of two-body decay near τ threshold are studied according to the special capacity of the BEPC II accelerator and the BESIII detector. Explicitly presented are the transformations of energy and momentum of hadronic particles between different reference frames, and the corresponding distributions. A brand new method is proposed to obtain the energy spread of the accelerator by fitting the energy distribution of hadron from τ semi-leptonic decays.

Key words kinematics, τ threshold, energy distribution, energy spread

PACS 13.35.Dx, 13.66.De, 02.70.Uu

1 Introduction

The τ -charm energy region is unique at the boundary between the perturbative and non-perturbative regime of quantum chromodynamics (QCD) and therefore becomes a bonanza for high energy physics. Since its completion in 1989, the Beijing Electron-Positron Collider (BEPC) and Beijing Spectrometer (BES) have been in operation successfully until 2004. A great many interesting and exciting physics topics were studied [1, 2], among which was the precise measurement of τ mass.

To meet the requirement of high precision τ and charm decay data, both the BEPC and the BES have been upgraded into BEPC II [3] and BESIII [4], respectively. The designed peak luminosity is $10^{33} \text{ cm}^{-2}\cdot\text{s}^{-1}$ optimized at a beam energy of 1.89 GeV, which is the highest luminosity accelerator in the τ -charm region ever planned [5]. The new machine could produce up to 1.2×10^7 τ -pairs per year [6], but this is not the crucial advantage of the τ -charm factory for τ physics. Today, the B-factories have samples of over 10^9 τ -pair events [7] and the LHC will produce 10^{12} τ -pairs per year even at low luminosity [8]. The real advantage for τ physics at BESIII is that the τ -pair is produced at threshold, which al-

lows the experiments to analyze many aspects of the τ decays with low systematic uncertainty.

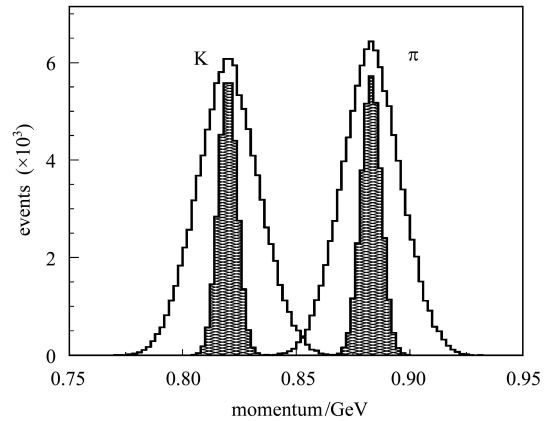


Fig. 1. Momentum distributions for $\tau \rightarrow (\pi, K)\nu$ decays. The hatched histograms indicate the distributions only with the effect of momentum resolution of the detector ($\delta_p = 0.5\%p$), while the blank histograms show both the beam energy spread ($\Delta_E = 1.2 \text{ MeV}$) and momentum resolution effects. The distributions are arbitrarily normalized.

The τ mass measurement at BES was performed near the τ threshold more than two decades ago. A precision of 0.2 MeV was achieved, which was the

Received 2 February 2010, Revised 24 March 2010

* Supported by National Natural Science Foundation of China (10491303, 10775412, 10825524, 10935008), Instrument Developing Project of Chinese Academy of Sciences (YZ200713), Major State Basic Research Development Program (2009CB825206) and Knowledge Innovation Project of Chinese Academy of Sciences (KJCX2-YW-N29)

1) E-mail: moxh@ihep.ac.cn

©2010 Chinese Physical Society and the Institute of High Energy Physics of the Chinese Academy of Sciences and the Institute of Modern Physics of the Chinese Academy of Sciences and IOP Publishing Ltd

most accurate result at that time [9, 10]. Even recently, few experiments reach compatible accuracy to the previous BES result [11–14]. At the forthcoming detector, as well as an even higher precision τ mass measurement, more results are expected. One of them is a high accuracy branching ratio measurement [8]. For such kinds of measurement, the kinematics in the vicinity of the τ threshold provides a unique advantage. As shown in the hatched histograms in Fig. 1, if the τ -pair is produced at threshold, $\sqrt{s} = 3.554$ GeV, the momentum distributions of π and K particles from $\tau^- \rightarrow \pi^- \nu$ and $K^- \nu$ separate from each other fairly well. It seems that no particle identification is needed under such circumstances. However, in actual data taking, the beam energy spread due to the accelerator has to be taken into account, which widens the momentum distributions considerably, as shown in the blank histograms in Fig. 1. Such broadness will cause π/K cross contamination, then degrade the accuracy of the branching ratio measurement. There are other sources that will change the kinematics of the τ decay. Therefore, it is necessary to understand theoretically various effects on the kinematics of the decay particle near the τ threshold at the BESIII experiment. It will provide information for an understanding of the characteristics of decay particles and for further experimental measurements.

Since more than half of τ decays can be summarized as two-body or quasi-two-body decay as $\tau^\pm \rightarrow$

$\nu_\tau h^\pm$, where h denotes the hadronic system which might further fragment into several mesons [8, 15], this paper is devoted to the kinematics of two-body decay near τ threshold. Furthermore, to simplify mathematical deduction and emphasize physical meaning, only $\pi\nu$ and $K\nu$ final states are used as special examples.

2 Energy-momentum transformation

2.1 Three reference frames

First of all, three reference frames defined are those needed for the study that follows.

1) The Colliding Beam System (CBS) is defined as the frame where an electron and a positron of equal absolute value of momentum collide with a crossing angle (denoted as 2α , $\alpha = 11$ mrad), as shown in Fig. 2(a).

2) The Center-of-Momentum System (CMS) is defined as the frame where the total momentum of the system is zero¹⁾. For our study, the CMS contains a pair of τ -leptons. Each of them has a momentum with equal magnitude but opposite sign. If there is no crossing angle between the electron and positron beams, viz. $\alpha = 0$, the CMS coincides with the CBS.

3) The Tau-Rest System (TRS) is defined as the frame where the τ -lepton is at rest. Within this system, the particle will have mono-energetic momentum for two-body decays, such as $\tau \rightarrow \pi\nu$ or $\tau \rightarrow K\nu$.

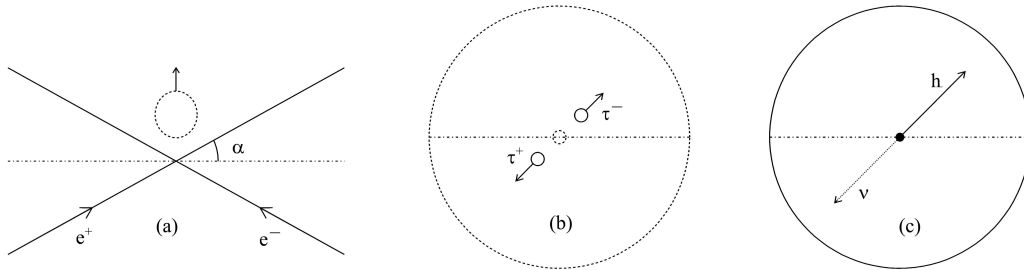


Fig. 2. Three reference frames: (a) the colliding beam system where the dashed circle denotes the whole boosted system due to the collision angle; (b) the center-of-momentum system where τ^\pm fly along the same line but opposite directions if just at the τ -pair threshold, two τ leptons produced at rest at the center are denoted by a small dashed circle; (c) the tau-rest system where the τ -lepton is at rest and denoted by a solid point. A two-body decay process $\tau \rightarrow h\nu$ is displayed in (c), where the solid line indicates the hadron track while the dotted line denotes the neutrino. In all plots, the dot-dashed line indicates the horizontal beam pipe.

Following the generic relativistic convention, E denotes the energy, p stands for the magnitude of the vector momentum, which is written as the bold type of the corresponding symbol \mathbf{p} ($p = |\mathbf{p}|$). (Hereafter,

the normal letter will represent the magnitude of the corresponding bold letter). Energy and corresponding momentum satisfy the relation

$$E^2 = p^2 + m^2, \quad \text{or} \quad p^2 = E^2 - m^2, \quad (1)$$

¹⁾ Conventionally, the Center-of-Momentum System is also called the Center-of-Mass System. However, in relativistic particle kinematics, we follow the nomenclature in Refs. [16, 17].

where m is the mass of the particle. The sub-scripts “ \parallel ” and “ \perp ” denote the parallel and perpendicular components of momentum, respectively.

If there are two reference systems Σ and Σ' , the energy and momentum in each of them are respectively denoted as (E, \mathbf{p}) and (E', \mathbf{p}') , and see from Σ , Σ' has velocity $\boldsymbol{\beta}$, then the relation between (E', \mathbf{p}') and (E, \mathbf{p}) is expressed by the Lorentz transformation,

$$\begin{pmatrix} E' \\ p'_{\parallel} \end{pmatrix} = \begin{pmatrix} \gamma & -\gamma\boldsymbol{\beta} \\ -\gamma\boldsymbol{\beta} & \gamma \end{pmatrix} \begin{pmatrix} E \\ p_{\parallel} \end{pmatrix}, \quad p'_{\perp} = p_{\perp}, \quad (2)$$

where $\gamma = (1 - \beta^2)^{-1/2}$, and p_{\parallel} (p_{\perp}) are the components of \mathbf{p} parallel (perpendicular) to $\boldsymbol{\beta}$. The corresponding inverse transformation reads

$$\begin{pmatrix} E \\ p_{\parallel} \end{pmatrix} = \begin{pmatrix} \gamma & \gamma\boldsymbol{\beta} \\ \gamma\boldsymbol{\beta} & \gamma \end{pmatrix} \begin{pmatrix} E' \\ p'_{\parallel} \end{pmatrix}, \quad p_{\perp} = p'_{\perp}. \quad (3)$$

Eqs. (2) and (3) are standard forms utilized in the high energy community.

For clearness and convenience, some symbols to be used afterwards are tabulated in Table 1. As far as angular variables are concerned, in the CMS, the direction of motion of the positron along the beam pipe (say, the direction from the left to the right along the dot-dashed line in Fig. 2(b)) and in the TRS, the direction of motion of the τ lepton, are chosen respectively as both the positive z -axis and the polar-axis.

Table 1. Notations for various variables and quantities.

symbol	meaning
E_e	beam energy
\mathbf{p}_e	beam momentum
W	energy of the CMS
E_{α}	energy of the CMS in the CBS
\mathbf{p}_{α}	momentum of the CMS in the CBS
\tilde{E}	energy of decay particle in the CBS
$\tilde{\mathbf{p}}$	momentum of decay particle in the CBS
E_c	energy of τ in the CMS
\mathbf{p}_c	momentum of τ in the CMS
E	energy of decay particle in the CMS
\mathbf{p}	momentum of decay particle in the CMS
θ	azimuthal angle of decay particle in the CMS
ϕ	polar angle of decay particle in the CMS
E_{τ}	energy of τ in the TRS
\mathbf{p}_{τ}	momentum of τ in the TRS
E^*	energy of decay particle in the TRS
\mathbf{p}^*	momentum of decay particle in the TRS
θ^*	azimuthal angle of decay particle in the TRS
ϕ^*	polar angle of decay particle in the TRS

In addition, we introduce a function f to denote the distribution of the differential cross section,

$$f(\mathbf{x}) = \frac{d\sigma}{d\mathbf{x}}, \quad (4)$$

where \mathbf{x} indicates the variable vector. The transformation between variables \mathbf{x} and \mathbf{y} is realized through the calculation of Jacobian $\partial\mathbf{y}/\partial\mathbf{x}$, viz.

$$f(\mathbf{x}) = f(\mathbf{y}) \cdot \left| \frac{\partial\mathbf{y}}{\partial\mathbf{x}} \right|. \quad (5)$$

2.2 Lorentz transformation

Now we consider the Lorentz transformation between different systems and start from the TRS. In the TRS, τ is at rest, therefore $\mathbf{p}_{\tau} = 0$ and $E_{\tau} = m_{\tau}$ (the τ mass). For two-body decay in the TRS, the momenta of two decay particles have the same magnitude but opposite direction. Notice that the neutrino mass is zero, it is immediately obtained

$$p^* = \frac{m_{\tau}^2 - m_h^2}{2m_{\tau}}, \quad E^* = \frac{m_{\tau}^2 + m_h^2}{2m_{\tau}}, \quad (6)$$

where subscript h indicates the hadron, that is a pion or kaon for the current analysis.

Seeing from the CMS, the TRS has a velocity $\boldsymbol{\beta}_c$, so applying the Lorentz transformation Eq. (2), the relation between the CMS and the TRS can be acquired. We define

$$\boldsymbol{\beta}_c = \frac{\mathbf{p}_c}{E_c}, \quad \gamma_c = \frac{E_c}{m_{\tau}}, \quad \boldsymbol{\eta}_c = \frac{\mathbf{p}_c}{m_{\tau}}. \quad (7)$$

Here, a new quantity $\boldsymbol{\eta}_c = \gamma_c \boldsymbol{\beta}_c$ is introduced for the convenience of derivation. With the help of $\boldsymbol{\eta}_c$, it can be acquired as

$$\mathbf{p}_{\parallel} = \frac{\mathbf{p} \cdot \boldsymbol{\eta}_c}{\eta_c^2} \boldsymbol{\eta}_c, \quad \mathbf{p}_{\perp} = \mathbf{p} - \mathbf{p}_{\parallel}. \quad (8)$$

Using Eq. (2),

$$\begin{aligned} E^* &= \gamma_c E - \boldsymbol{\eta}_c \cdot \mathbf{p}, \\ p'_{\parallel} &= \gamma_c p_{\parallel} - \eta_c E, \\ p'_{\perp} &= p_{\perp}. \end{aligned} \quad (9)$$

Again, notice the definition of $\boldsymbol{\eta}_c$ and use the relation in Eq. (8), it is acquired finally

$$\begin{cases} E^* = \frac{1}{m_{\tau}} \cdot (E_c E - \mathbf{p}_c \cdot \mathbf{p}), \\ \mathbf{p}^* = \mathbf{p} - \frac{\mathbf{p}_c}{m_{\tau}} \cdot \left(E - \frac{\mathbf{p}_c \cdot \mathbf{p}}{E_c + m_{\tau}} \right). \end{cases} \quad (10)$$

Using Eq. (3), the inverse transformation can be obtained analogously,

$$\begin{cases} E = \frac{1}{m_{\tau}} \cdot (E_c E^* + \mathbf{p}_c \cdot \mathbf{p}^*), \\ \mathbf{p} = \mathbf{p}^* + \frac{\mathbf{p}_c}{m_{\tau}} \cdot \left(E^* + \frac{\mathbf{p}_c \cdot \mathbf{p}^*}{E_c + m_{\tau}} \right). \end{cases} \quad (11)$$

Seeing from the CBS, the CMS has velocity $\boldsymbol{\beta}_{\alpha}$, then

$$\boldsymbol{\beta}_{\alpha} = \frac{\mathbf{p}_{\alpha}}{E_{\alpha}}, \quad \gamma_{\alpha} = \frac{E_{\alpha}}{m_{\tau}}, \quad \boldsymbol{\eta}_{\alpha} = \frac{\mathbf{p}_{\alpha}}{m_{\tau}}. \quad (12)$$

With a similar technique, the transformation from the CBS to the CMS reads

$$\begin{cases} E = \frac{1}{m_\tau} \cdot (E_\alpha \tilde{E} - \mathbf{p}_\alpha \cdot \tilde{\mathbf{p}}), \\ \mathbf{p} = \tilde{\mathbf{p}} - \frac{\mathbf{p}_\alpha}{m_\alpha} \cdot \left(\tilde{E} - \frac{\mathbf{p}_\alpha \cdot \tilde{\mathbf{p}}}{E_\alpha + m_\alpha} \right), \end{cases} \quad (13)$$

and the transformation from the CMS to the CBS is as follows,

$$\begin{cases} \tilde{E} = \frac{1}{m_\tau} \cdot (E_\alpha E - \mathbf{p}_\alpha \cdot \mathbf{p}), \\ \tilde{\mathbf{p}} = \mathbf{p} + \frac{\mathbf{p}_\alpha}{m_\alpha} \cdot \left(E + \frac{\mathbf{p}_\alpha \cdot \mathbf{p}}{E_\alpha + m_\alpha} \right). \end{cases} \quad (14)$$

Experimentally, E_e and \mathbf{p}_e are provided by the accelerator, before collision, $E_\alpha = 2E_e$ and $\mathbf{p}_\alpha = 2\mathbf{p}_e$, after collision,

$$E_\alpha = 2E_e, \quad \mathbf{p}_\alpha = 2p_e \sin \alpha \hat{\mathbf{x}}, \quad (15)$$

where $\hat{\mathbf{x}}$ indicates the unity vector along the x -direction (the direction vertical to that of the beam pipe in the horizontal plane; refer to Fig. 2). Notice the relation $E_e = \sqrt{p_e^2 + m_e^2}$ and neglecting the electron mass m_e , $p_e \approx E_e$, so from Eq. (15), $\mathbf{p}_\alpha \approx E_\alpha \sin \alpha \hat{\mathbf{x}}$; then Eq. (12) becomes

$$\beta_\alpha = \sin \alpha \hat{\mathbf{x}}, \quad \gamma_\alpha = \frac{1}{\cos \alpha}, \quad \boldsymbol{\eta}_\alpha = \tan \alpha \hat{\mathbf{x}}. \quad (16)$$

In the CMS, the total momentum is zero and the total energy is denoted as W . So with the help of Eq. (16), the Lorentz transformation between the CMS and the CBS leads to the relation

$$E_\alpha = \gamma_\alpha W, \quad \text{or} \quad W = E_\alpha \cos \alpha. \quad (17)$$

If $\alpha = 0$, then $W = E_\alpha$. In other words, the CBS coincides with the CMS, just as expected.

3 Distribution transformation

3.1 Boost

In the CMS, if the energy is just at τ threshold, that is $W = 2m_\tau$, two τ leptons are produced at rest. The momentum of the two-body hadron is fixed as given in Eq. (6). However, when the energy increases, the distribution of momentum will expand accordingly. The range of momentum distribution is determined by the difference between the maximum and minimum momenta, which are obtained when the decay hadron flies along or opposite to the boost direction, i.e. parallel or anti-parallel to β_c or β_α (in such a case, the perpendicular component of momentum is zero). By virtue of Eq. (3),

$$\begin{pmatrix} E_+ \\ p_+ \end{pmatrix} = \begin{pmatrix} \gamma_c & \gamma_c \beta_c \\ \gamma_c \beta_c & \gamma_c \end{pmatrix} \begin{pmatrix} E^* \\ p^* \end{pmatrix}, \quad (18)$$

and

$$\begin{pmatrix} E_- \\ -p_- \end{pmatrix} = \begin{pmatrix} \gamma_c & \gamma_c \beta_c \\ \gamma_c \beta_c & \gamma_c \end{pmatrix} \begin{pmatrix} E^* \\ -p^* \end{pmatrix}. \quad (19)$$

Here, the minus sign before the momentum is added to keep p_- and/or p^* positive numbers. Consequently, in the CBS,

$$\begin{pmatrix} \tilde{E}_+ \\ \tilde{p}_+ \end{pmatrix} = \begin{pmatrix} \gamma_\alpha & \gamma_\alpha \beta_\alpha \\ \gamma_\alpha \beta_\alpha & \gamma_\alpha \end{pmatrix} \begin{pmatrix} E_+ \\ p_+ \end{pmatrix}, \quad (20)$$

and

$$\begin{pmatrix} \tilde{E}_- \\ -\tilde{p}_- \end{pmatrix} = \begin{pmatrix} \gamma_\alpha & \gamma_\alpha \beta_\alpha \\ \gamma_\alpha \beta_\alpha & \gamma_\alpha \end{pmatrix} \begin{pmatrix} E_- \\ -p_- \end{pmatrix}. \quad (21)$$

Using the above equations, the range of momentum is obtained,

$$\Delta p = \tilde{p}_+ - \tilde{p}_- = 2(\gamma_\alpha \beta_\alpha \gamma_c + \gamma_c \beta_c \gamma_\alpha) E^*. \quad (22)$$

The variations in Δp with energy W are shown in Fig. 3.

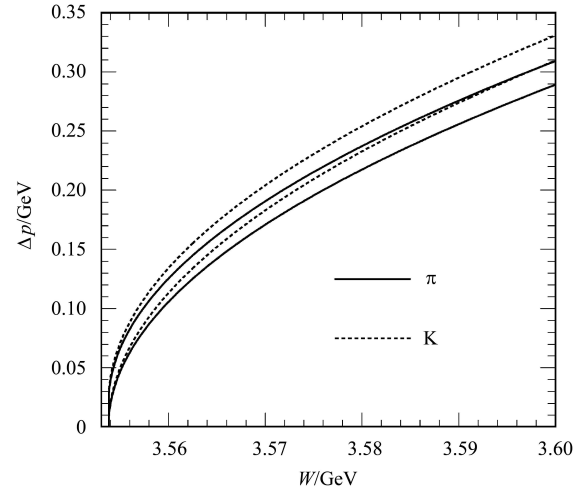


Fig. 3. Δp as a function of energy W pion (solid line) and kaon (dashed line) momenta. The lines below for pion and kaon correspond to the case $\alpha = 0$, which amounts to the boost effect merely in the CMS.

Some remarks are in order here. First, it is seen that for the CBS the effect due to the crossing angle of the colliding beam is fixed (along the $\hat{\mathbf{x}}$ direction) and is comparatively small (for $\alpha = 11$ mrad, $\cos \alpha \approx 1$ and $\sin \alpha \approx 0$), which can be described by a definite Lorentz transformation. Therefore, in the following study, such an effect is neglected and the discussion is focused on the kinematics in the CMS. Second, in the vicinity of the τ threshold, the velocity of the particle in the TRS (denoted as $v^* = p^*/E^*$) is usually greater than the velocity of the reference,

such as β_c or β_α . When $v^* = \beta_c$, it can be worked out that $W_\pi = 22.8$ GeV and $W_K = 6.9$ GeV. So for pion and kaon, as long as $W < W_\pi$ or $W < W_K$, then $v^* > \beta_c$. As in the τ -charm region with W usually less than 5 GeV, the condition $v^* > \beta_c$ is always satisfied. Third, as shown in Fig. 3, the momentum range expands rather rapidly as the energy increases, which implicates the great impact of energy spread on the momentum distribution as mentioned in the introduction. Next we consider this problem in more detail.

3.2 Energy spread

In this section, the energy spread effect on the distribution of the final state hadron energy instead of that of the momentum is considered. The calculation for scalar energy is much easier than that for momentum, which is a vector.

We start from the TRS, where the angular distribution of the hadron is isotropic,

$$f(\cos\theta^*, \phi^*) = \frac{1}{4\pi}. \quad (23)$$

Integrating with respect to $d\phi^*$,

$$f(\cos\theta^*) = \frac{1}{2}. \quad (24)$$

By virtue of the basic transformation law [17],

$$f(E) = f(\cos\theta^*) \frac{\partial \cos\theta^*}{\partial E}.$$

From Eq. (11),

$$E = \frac{1}{m_\tau} \cdot (E_c E^* + p_c p^* \cos\theta^*), \quad (25)$$

$\partial \cos\theta^* / \partial E = m_\tau / (p_c p^*)$ is immediately obtained, then

$$f(E) = \frac{m_\tau}{2p_c p^*}. \quad (26)$$

The independence of $f(E)$ on E indicates that E has equal probability along any spatial direction in the CMS without regarding the energy spread effect.

Since $-1 \leq \cos\theta^* \leq 1$, from Eq. (25), the maximum and minimum of E are obtained at $\theta^* = 0$ and π , that is,

$$E_{\max} = \frac{1}{m_\tau} \cdot (E_c E^* + p_c p^*), \quad E_{\min} = \frac{1}{m_\tau} \cdot (E_c E^* - p_c p^*). \quad (27)$$

With E_{\max} and E_{\min} , Eq. (26) can be recast in an explicitly energy-dependent form,

$$f(E) = \frac{m_\tau}{2p_c p^*} \cdot [\Theta(E - E_{\min}) - \Theta(E - E_{\max})], \quad (28)$$

where Θ is the step function and the value field of E ranges from $-\infty$ to $+\infty$.

Now consider the energy spread effect. In the CMS, notice $W = 2E_c$, or

$$E_c = \frac{W}{2}, \quad p_c = \frac{W}{2} \sqrt{1 - \frac{4m_\tau^2}{W^2}}. \quad (29)$$

Here, W is subject to the energy spread effect, that is to say, W is actually a random number that obeys the Gaussian distribution

$$f_G(W) = \frac{\Theta(W - 2m_\tau)}{\sqrt{2\pi}\Delta} \exp\left[-\frac{(W - W_0)^2}{2\Delta^2}\right], \quad (30)$$

where Δ is the energy spread¹⁾, determined by the accelerator performance, and W_0 is the nominal energy value. Therefore, in the light of Eq. (25), E is the function of two random variables $\cos\theta^*$ and W (through E_c by Eq. (29)). To acquire the distribution of E from those of $\cos\theta^*$ and W , the variable transformation technique in probability theory is adopted [18]. For clearness, $\cos\theta^*$ is denoted as x , then

$$f(W, x) = f_G(W) \cdot f(x). \quad (31)$$

Here, W and x are two independent random variables. $f_G(W)$ is given by Eq. (30), and $f(x)$ by

$$f(x) = \frac{\Theta(x+1) - \Theta(x-1)}{2}. \quad (32)$$

The distribution with new variables E and x can be related to the previous one by Jacobian determinant,

$$g(E, x) = f(W, x) \left| J \left(\frac{W, x}{E, x} \right) \right|, \quad (33)$$

with

$$J \left(\frac{W, x}{E, x} \right) = \begin{vmatrix} \frac{\partial W}{\partial E} & \frac{\partial W}{\partial x} \\ \frac{\partial x}{\partial E} & \frac{\partial x}{\partial x} \end{vmatrix} = \frac{\partial W}{\partial E}. \quad (34)$$

Integrating with respect to x , finally the distribution for E is obtained as

$$\begin{aligned} g(E) &= \int_{-\infty}^{\infty} g(E, x) dx \\ &= \int_{-\infty}^{\infty} dx f[W(E), x] \left| \frac{\partial W}{\partial E} \right|, \end{aligned} \quad (35)$$

with

$$\begin{aligned} W &= \frac{2m_\tau}{(E^*)^2 - (xp^*)^2} \cdot \left[EE^* \right. \\ &\quad \left. + xp^* \sqrt{E^2 + (xp^*)^2 - (E^*)^2} \right], \end{aligned} \quad (36)$$

and

$$\frac{\partial W}{\partial E} = \frac{2m_\tau}{(E^*)^2 - (xp^*)^2} \cdot \left[E^* + \frac{xp^* E}{\sqrt{E^2 + (xp^*)^2 - (E^*)^2}} \right]. \quad (37)$$

1) According to Ref. [5], $\Delta(\text{MeV}) = 0.386E_e^2(\text{GeV}^2)$, so at τ threshold, $\Delta \approx 1.22$ MeV.

The detailed derivation of Eqs. (36) and (37) can be found in the Appendix.

Figure 4 shows three energy distributions corresponding to different nominal energies W_0 . The energy spread ($\Delta = 1.2$ MeV) effect has been taken into account. The solid line indicates the distribution which is just at τ threshold ($W_0 = 2m_\tau$); the dashed line indicates that the distribution is around two Δ s above the τ threshold ($W_0 = 2m_\tau + 2\Delta$); and the dot-dashed line indicates that the distribution is around five Δ s above τ threshold ($W_0 = 2m_\tau + 5\Delta$). The broadness of energy distribution is obvious with the increase in center-of-energy.

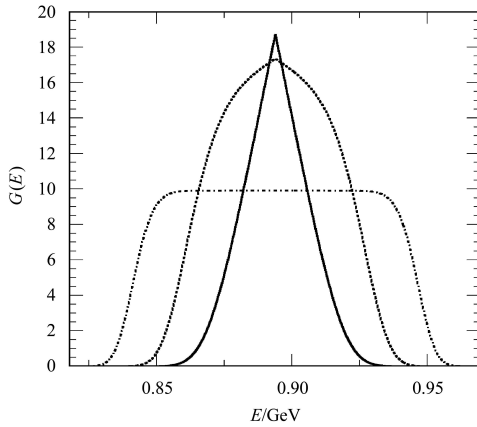


Fig. 4. Energy distribution ($g(E)$) at different nominal energies (W_0) with the effect due to the energy spread ($\Delta = 1.2$ MeV). The solid line indicates $W_0 = 2m_\tau$, the dashed line $W_0 = 2m_\tau + 2\Delta$, and the dot-dashed line $W_0 = 2m_\tau + 5\Delta$. Here, the $\pi\nu$ final state is considered and E indicates the energy of π in the CMS.

3.3 Momentum resolution

Momentum resolution is another experimental effect which should be taken into account. For the nominal momentum p_0 , the actual momentum obeys a Gaussian distribution,

$$f(p, p_0) = \frac{1}{\sqrt{2\pi}\delta} \exp\left[-\frac{(p-p_0)^2}{2\delta^2}\right], \quad (38)$$

where the δ is momentum resolution. Noting the relativistic relation between energy and momentum as given in Eq. (1) and using the chain rule for distribution transformation [17], it is found that

$$\begin{aligned} f(E, E_0) &= f[p(E), p_0(E_0)] \cdot \frac{\partial p}{\partial E} \\ &= \frac{1}{\sqrt{2\pi}\delta} \exp\left[-\frac{(\sqrt{E^2 - m_h^2} - p_0)^2}{2\delta^2}\right] \\ &\quad \times \frac{E}{\sqrt{E^2 - m_h^2}}, \end{aligned} \quad (39)$$

where $p_0 = \sqrt{E_0^2 - m_h^2}$.

In the light of conditional probability theory [18], the synthetic density of $g(E)$ in Eq. (35) and $f(E, E_0)$ in Eq. (39) can be obtained, viz.

$$G(E) = \int_{-\infty}^{+\infty} g(z) \cdot f(E, z) dz. \quad (40)$$

In the actual calculation, the up and low limits are taken as a few times δ away from the center value of p_0 .

3.4 Fitting energy spread

The energy spread is an important parameter for both the accelerator and the detector but is difficult to measure accurately. Around the τ threshold, the energy spread is usually extrapolated from those of J/ψ and ψ' [10], which are obtained by fitting the corresponding resonance parameters [19, 20]. Here we present a brand new method to determine the energy spread in the vicinity of the τ threshold.

As seen from the analyses in the previous sections, the energy spread effect will broaden the energy distribution considerably and therefore weaken the advantage of kinematics near the τ threshold. On the other hand, the prominent effect of the energy spread on the energy distribution makes it possible to extract the information of energy spread directly from the energy distribution. To confirm this idea, we resort to a Monte Carlo (MC) simulation to simulate two-body τ -lepton decay near the threshold. For simplification, we only consider two important experimental parameters: the energy spread of the BEPC II ($\Delta = 1.2$ MeV) [3, 5] and the momentum resolution of the BESIII ($\delta/p = 0.5\%$) [4].

Our simulations are classified into four steps. Firstly, for a nominal c.m. energy W_0 , the experimental energy is obtained by sampling

$$W = W_0 + \Delta \cdot \xi,$$

where ξ is a random number of standard normal distribution $N(0,1)$. It should be noted that the kinematic requirement $W \geq 2m_\tau$ must be added as indicated by the step function in Eq. (30).

Secondly, in the TRS, E^* and p^* are given by Eq. (6). As to \mathbf{p}^* , its components are obtained as follows,

$$\begin{aligned} p_x^* &= p^* \sin\theta^* \cos\phi^*, \\ p_y^* &= p^* \sin\theta^* \sin\phi^*, \\ p_z^* &= p^* \cos\theta^*, \end{aligned}$$

where ϕ^* has a uniform distribution between 0 and

2π , and $\cos\theta^*$ has a uniform distribution¹⁾ between -1 and $+1$.

Thirdly, E_c and p_c can be obtained from W according to Eq. (29). In the CMS, \mathbf{p}_c distributes uniformly for ϕ_c and $\cos\theta_c$ ²⁾, that is,

$$\begin{aligned} p_{cx} &= p_c \sin\theta_c \cos\phi_c, \\ p_{cy} &= p_c \sin\theta_c \sin\phi_c, \\ p_{cz} &= p_c \cos\theta_c, \end{aligned}$$

where the subscript c indicates the CMS. With (E_c, \mathbf{p}_c) and (E^*, \mathbf{p}^*) , according to Eq. (11), the energy E and momentum \mathbf{p} in the CMS are acquired, then

$$p = \sqrt{p_x^2 + p_y^2 + p_z^2}.$$

Finally, consider the momentum resolution effect.

The momentum p obtained in the third step is treated as the nominal momentum and denoted as p_0 , then the measured momentum p is obtained by sampling

$$p = p_0 + \delta \cdot \zeta,$$

where ζ is a random number of standard normal distribution $N(0, 1)$. The measured energy is then calculated as $E = \sqrt{p^2 + m_h^2}$.

Figure 5 displays the fit results of energy distribution at different c.m. energy with effects due to both the energy spread and the momentum resolution. The density depicted in Eq. (40) is used as the fitting function³⁾ and three parameters (Δ , δ and an overall normalization factor) are set free in the fitting. The minimization is realized by the MINUIT package [24].

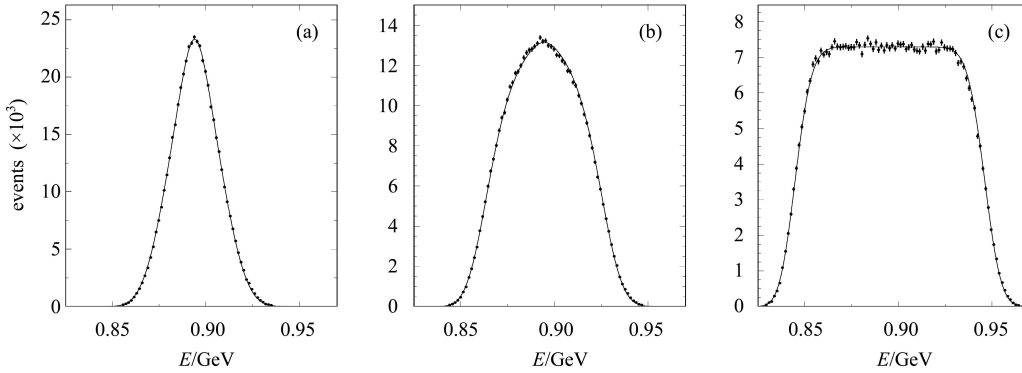


Fig. 5. Energy distributions at different centers-of-energy with effects due to the energy spread ($\Delta = 1.2$ MeV) and momentum resolution ($\delta/p = 0.5\%$). The solid lines are the best fit results while the dots with error bars are the simulated data. The produced events are 0.5M for all three c.m. energies: (a) $W_0 = 2m_\tau$, (b) $W_0 = 2m_\tau + 2\Delta$, and (c) $W_0 = 2m_\tau + 5\Delta$. Here, the $\pi\nu$ final state is considered and E indicates the energy of π in the CMS.

The results relevant to the fits are summarized in Table 2, where the statistical error is solely the value from the minimization fitting while the systematic only indicates the deviation of the fitted value from the input in the MC simulation. As to the relative error (ν), it is calculated as follows: for certain variable y representing c.m. energy W_0 or energy spread

Δ , the fitted value is denoted as y_{fit} and the input MC value as y_{MC} , then the relative difference

$$\nu_y \equiv \frac{|y_{\text{fit}} - y_{\text{MC}}|}{y_{\text{MC}}}.$$

Scrutinizing the results quoted in Table 2 reveals the following two points. Firstly, with the increase

1) In the TRS, the distribution of hadron from τ decay has the form [21]

$$\frac{d\sigma}{d\cos\theta^*} = 1 + \kappa_h \cos\theta^*,$$

where $\kappa = +1$ or -1 , which corresponds to a 100% positive or negative polarized τ lepton. However, in our experiment, the unpolarized particles are measured and on average the distribution for the τ -lepton decay is uniform.

2) The differential cross section for the τ -pair in the CMS is an analogue of the μ -pair [22],

$$\frac{d\sigma}{d\Omega} = \frac{\alpha^2}{4W^2} \sqrt{1 - \frac{m_\tau^2}{E_c^2}} \left[\left(1 + \frac{m_\tau^2}{E_c^2}\right) + \left(1 - \frac{m_\tau^2}{E_c^2}\right) \cos^2\theta_c \right].$$

At the τ threshold, $E_c \approx m_\tau$, therefore the dependence of $d\sigma/d\Omega$ on $\cos^2\theta_c$ can be neglected. In other words, a uniform distribution could be used in the vicinity of τ threshold in our study. As a matter of fact, the spatial distribution of \mathbf{p} has no effect on our analysis, since here only the magnitude of \mathbf{p} is of concern.

3) The two dimensional integration is realized by the CERN library program [23].

Table 2. The relative errors of the statistical and systematic about c.m. energy (W_0) and energy spread (Δ) for different numbers of produced events ($N_{\text{evt.}}$) at different energy points. Here, the statistical error (the first number for each item) is solely the value from the minimization fitting while the systematic error (the second number for each item) only indicates the deviation of the fitted value from the input in the MC simulation.

$N_{\text{evt.}}$	$2m_\tau$	$2m_\tau + 2\Delta$	$2m_\tau + 5\Delta$
c.m. energy ($10^{-5}/10^{-5}$)			
5k	6.5/2.4	1.3/1.5	2.2/3.4
10k	4.4/4.8	1.0/0.0	1.6/1.1
0.5M	0.6/3.2	0.1/4.0	0.2/2.0
energy spread ($10^{-2}/10^{-2}$)			
5k	9.8/7.3	5.7/9.4	9.6/14
10k	6.4/9.2	3.9/5.1	5.9/5.0
0.5M	0.9/5.1	0.5/2.3	0.8/2.8

in the data sample, the statistical errors decrease correspondingly while the case is more complex for the systematic errors. For the fit of W_0 , the deviation remains almost the same regardless of the size of the sample. For Δ , the deviation is commonly greater than the statistical precision and the decrease in systematic uncertainty is rather slow compared with the statistical one. Secondly, for the W_0 fit, there seems to be no optimal point for systematic deviation, that is to say any energy point will yield almost the same accuracy; while as far as the statistical error is concerned, the energy point $W_0 = 2m_\tau + 2\Delta$ seems more favorable. For Δ fit, the point $W_0 = 2m_\tau + 2\Delta$ is also favorable, which provides more accurate results. In other words, for energy spread measurement, neither the τ threshold nor the energy point far away from the threshold is optimal. Summarizing the above discussion, the results listed in Table 2 indicate¹⁾ that the optimal energy point for the fit should be

around ($2m_\tau + 2\Delta$). In addition, from the experimental point of view, the data sample of the size of 10 k is reasonable, which could accommodate the energy spread value with the uncertainty at the level of five percent²⁾. Such accuracy is much better than the present experimental measurement whose uncertainty is at the level of 10% to 15% [25, 26].

4 Summary

In this paper, we analyze in detail the kinematics for the two-body decay of the τ lepton near its threshold in e^+e^- annihilation at the BESIII. The experimental conditions are taken into account, the transformations of energy and momentum between different reference frames are studied and special transformation formulas are presented.

Based on the transformation formulas, both the energy spread and the momentum resolution are taken into consideration for the energy distribution of hadron from the τ decay. The analytic integral expression for energy distribution is firstly obtained, which can be used for fitting the experimental energy distribution.

The most important application of the analytical formula is that we can fit the measured energy distribution of the particle from the τ decays to obtain the value of the energy spread. The Monte Carlo simulation technique is adopted to confirm our idea and to study the fit uncertainty relevant to the energy spread. The results indicate that, through minimization, the energy spread can be determined with an accuracy at the level of five percent.

The author gratefully acknowledges Professor ChangZheng Yuan for his constructive comments and valuable suggestions.

1) In order to fix the optimized energy point, more detailed studies are needed; e.g. the finer fit scan within the energy region [$2m_\tau, 2m_\tau + 5\Delta$] should be performed. In addition, more accurate Monte Carlo simulations which take into account all detector details should be utilized in order to obtain the practical conclusion.

2) Further study of the relation between momentum resolution and energy spread uncertainty indicates that the smaller the momentum resolution, the smaller is the systematic uncertainty of the energy spread.

Appendix A

Formulas

Starting from Eq. (25), noticing $x = \cos\theta^*$ and introducing variable $\rho = xp^*$, we immediately obtain

$$m_\tau E - E_c E^* = p_c \rho.$$

Utilizing the relation of Eq. (29) and squaring both sides of the above equation lead to

$$(E^{*2} - \rho^2)W^2 - 4m_\tau E E^* W + 4m_\tau (E^2 + \rho^2) = 0. \quad (\text{A1})$$

This quadratic equation for W has two solutions:

$$W = \frac{2m_\tau}{E^{*2} - \rho^2} \cdot \left[E E^* \pm |x| p^* \sqrt{E^2 + \rho^2 - (E^*)^2} \right]. \quad (\text{A2})$$

Noticing the symmetry of the value field of x , two solutions of W could be expressed as an integrated one;

that is,

$$W = \frac{2m_\tau}{E^{*2} - \rho^2} \cdot \left[E E^* + \rho \sqrt{E^2 + \rho^2 - (E^*)^2} \right], \quad (\text{A3})$$

which recovers Eq. (36). Differentiating W with respect to E yields Eq. (37).

We know for certain E_c , E has a uniform distribution as indicated by Eq. (26) or Eq. (28). Moreover, noticing Eq. (27), it can be seen that the distribution is symmetric about the central value $\gamma_c E^*$ (with $\gamma_c = E_c/m_\tau$). Physically, such symmetry should be remained for density $g(E)$ in Eq. (35). Therefore, if the measured energy, denoted as E_{mea} , is greater than $\gamma_c E^*$, $E = E_{\text{mea}}$; otherwise, $E = 2\gamma_c E^* - E_{\text{mea}}$. With this symmetric consideration, $\partial W/\partial E$ is always positive as well.

References

- 1 ZHENG Zhi-Peng, ZHU Yong-Sheng. BES: Electron-Positron Physics. Nanning: Guangxi Science and Technology Press, 1998 (in Chinese)
- 2 ZHENG Zhi-Peng, LI Wei-Guo. BESII: Electron-Positron physics. Hefei: University of Science and Technology of China Press, 2009 (in Chinese)
- 3 Preliminary Design Report of accelerator BEPC II. Second version, July, 2003 (in Chinese); <http://acc-center.ihep.ac.cn/bepcii/bepcii.htm>
- 4 Preliminary Design Report: The BESIII Detector, January, 2004
- 5 YUAN Chang-Zheng, ZHANG Bing-Yun, QIN Qing. HEP & NP, 2002, **26**: 1201–1208 (in Chinese)
- 6 WANG Y F. Int. J. Mod. Phys. A, 2006, **27**: 5371
- 7 Lafferty G D. Int. J. Mod. Phys. A, 2006, **27**: 5660
- 8 Atahl A. Int. J. Mod. Phys. A, 2006, **27**: 5667
- 9 BAI J Z et al. (BES collaboration). Phys. Rev. Lett., 1992, **69**: 3021
- 10 BAI J Z et al. (BES collaboration). Phys. Rev. D, 1996, **53**: 20
- 11 MO X H. Nucl. Phys. B Proc. Suppl., 2007, **163**: 132
- 12 Belous K et al. (The Belle collaboration). Phys. Rev. Lett., 2007, **99**: 011801
- 13 Aubert B et al. (The BaBar collaboration). Phys. Rev. D, 2007, **80**: 092005
- 14 Blinov V E et al. Nucl. Instrum. Methods A, 2009, **598**: 23–30
- 15 YAO W M et al. (Particle Data Group). J. Phys. G, 2006, **33**: 1
- 16 Byckling E, Kajantie K. Particle Kinematics. London: John Wiley & Sons, 1973
- 17 Hagedorn R. Relativistic Kinematics. Now York: W. A. Benjamin Inc., 1963
- 18 Brandt S. Data Analysis. Springer-Verlag New York Inc., 1999
- 19 BAI J Z et al. (BES collaboration). Phys. Lett. B, 1995, **355**: 374
- 20 BAI J Z et al. (BES collaboration). Phys. Lett. B, 2002, **550**: 24
- 21 Atahl A. Physics with Tau Leptons. Springer-Verlag Berlin Heidelberg, 2000
- 22 Peskin M E, Schroeder D V. An Introduction to Quantum Field Theory. Addison-Wesley Publishing Company, 1995
- 23 CERN Program Library Short Writeups. CERN, Geneva, 1996
- 24 MINUIT Reference Manual Version 92.1. CERN, Geneva, 1992
- 25 Klein R et al. Nucl. Instrum. Methods A, 1997, **384**: 293
- 26 Bondar A. Absolute Beam Energy Calibration at Novosibirsk, talk at Workshop on Future PRC/US cooperation in High Energy Physics, June 2006